Comparison of the Active-Site Design of Molybdenum Oxo-Transfer Enzymes by Quantum Mechanical Calculations

ARTICLE *in* INORGANIC CHEMISTRY · NOVEMBER 2014

Impact Factor: 4.76 · DOI: 10.1021/ic5010837 · Source: PubMed

2 AUTHORS:

Jilai Li
Jilin University
65 PUBLICATIONS **275** CITATIONS
SEE PROFILE

Ulf Ryde
Lund University
219 PUBLICATIONS **7,488** CITATIONS
SEE PROFILE

Inorganic Chemistry

Article

pubs.acs.org/IC

Comparison of the Active-Site Design of Molybdenum Oxo-Transfer Enzymes by Quantum Mechanical Calculations

Jilai Li[†,‡] and Ulf Ryde*[,†]

[†]Department of Theoretical Chemistry, Chemical Centre, Lund University, P.O. Box 124, SE-221 00 Lund, Sweden

[‡]State Key Laboratory of Theoretical and Computational Chemistry, Institute of Theoretical Chemistry, Jilin University, Changchun 130023, People's Republic of China

Supporting Information

ABSTRACT: There are three families of mononuclear molybdenum enzymes that catalyze oxygen atom transfer (OAT) reactions, named after a typical example from each family, viz., dimethyl sulfoxide reductase (DMSOR), sulfite oxidase (SO), and xanthine oxidase (XO). These families differ in the construction of their active sites, with two molybdopterin groups in the DMSOR family, two oxy groups in the SO family, and a sulfido group in the XO family. We have employed density functional theory calculations on cluster models of the active sites to understand the selection of molybdenum ligands in the three enzyme families. Our calculations show that the DMSOR active site has a much stronger oxidative power than the other two sites, owing to the extra molybdopterin ligand. However, the active sites do not seem to have been constructed to make the OAT reaction as exergonic as possible, but instead to keep the reaction free energy close to zero (to avoid excessive loss of energy), thereby making the reoxidation (SO and XO) or rereduction of the active sites (DMSOR) after the OAT reaction facile. We also show that active-site models of the three enzyme families can all catalyze the reduction of DMSO and that the DMSOR model does not give the lowest activation barrier. Likewise, all three models can catalyze the oxidation of sulfite, provided that the Coulombic repulsion between the substrate and the enzyme model can be overcome, but for this harder reaction, the SO model gives the lowest activation barrier, although the differences are not large. However, only the XO model can catalyze the oxidation of xanthine, owing to its sulfido ligand.

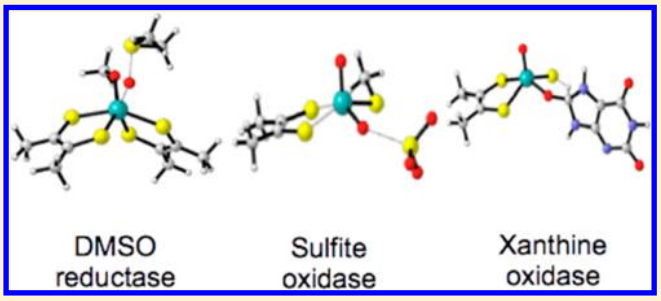

1. INTRODUCTION

Molybdenum (Mo) is the most common transition metal in seawater, with a concentration that is 100 times higher than that of, e.g., iron, owing to the solubility of its high-valent oxides.[1] Therefore, it is not surprising that it is involved in the metabolism of biological systems (it is the only essential 4d transition metal) and that enzymes containing this element are ubiquitous in Nature. Two groups of Mo enzymes are known. One is the nitrogenases, which contain a complicated $MoFe_7S_9C$ cluster in the active site. The other is a diverse group of enzymes that catalyze oxygen atom transfer (OAT) between the mononuclear Mo active site and various substrates, coupled with the transfer of two electrons. Many of these enzymes are involved in the biological carbon, nitrogen, and sulfur cycles. They all contain a specific dithiolene ligand, molybdopterin (MPT), which binds bidentately to Mo. In recent years, significant progress has been made in the understanding of their structures and mechanisms by experiments and theoretical calculations.[2,3]

The mononuclear Mo enzymes are classified into three families, based on the structure of the active site, viz., the dimethyl sulfoxide reductase (DMSOR), sulfite oxidase (SO), and xanthine oxidase (XO) families.[4−6] The active site of the DMSOR family contains two MPT cofactors bound to the Mo ion in a nearly planar fashion, one deprotonated side-chain O, S, or Se atom of serine, cysteine, or selenocysteine at the apical position, and, in the oxidized state, one oxo group[4] (Scheme 1). The active site of the SO family[3] has one MPT cofactor, one terminal oxo ligand in the apical position, a thiolate group of a cysteine residue, and, in the oxidized state, another terminal oxo ligand located at the equatorial position of a square-pyramidal geometry (Scheme 1).[7] In contrast, the equatorial cysteine ligand is replaced by a terminal sulfido ion and the equatorial oxy group is protonated to a hydroxyl group in the active site of XO[3,8] (Scheme 1). Mechanistic studies have demonstrated that most of the members of the XO family catalyze the hydroxylation of a diverse range of substrates by the insertion of an oxygen atom into a C−H bond. In contrast, the members of the DMSOR and SO families catalyze simple OAT reactions to or from various substrates.

The DMSOR family is the largest and most diverse of these three families of Mo enzymes. DMSOR catalyzes the OAT from dimethyl sulfoxide (DMSO) to the Mo^{IV} active site,

Received: May 13, 2014
Published: November 5, 2014

dx.doi.org/10.1021/ic5010837 | Inorg. Chem. 2014, 53, 11913−11924

Scheme 1. Structures of the Active Sites of the DMSOR (Left), SO (Middle), and XO (Right) Families of Mononuclear Mo OAT Enzymes[a]

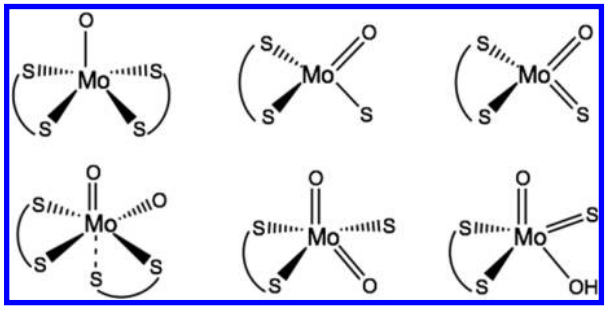

[a]The upper part shows the reduced states, and the lower part shows the corresponding oxidized states. ($^{S}_{S}$ represents the molybdopterin cofactor that coordinates to the Mo ion via its dithiolene side chain, −O and −S are amino acid side chains (Ser, Cys, or selenocysteine), =O and =S are oxo and sulfido ligands, and OH is a hydroxyl ligand.

yielding dimethyl sulfide (DMS) and Mo^{VI}=O. The reaction mechanism has been extensively studied.[2−4,7,9−20] There are also several experimental and computational studies of functional inorganic model complexes that perform a similar chemistry.[10] The studies have demonstrated that the reactivity is highly substrate dependent[21] and that the rate-determining step involves Mo−O bond formation and a two-electron transfer from the Mo^{IV} center to the substrate as the S−O bond breaks.[20]

The first theoretical study of DMSOR was performed by Webster and Hall.[12] Their B3LYP calculations on cluster models showed that the reaction proceeds via an associative transition state for the OAT with an energy barrier of 37 kJ/mol. A subsequent computational study by Mohr and co-workers gave a similar barrier height.[22] Thapper et al. studied also the binding of DMSO to the enzyme model and proposed a two-step mechanism based on a slightly different model system but a similar transition-state geometry.[13] These findings were confirmed also for the original model system by McNamara, Hernandez-Marin, and Ziegler, as well as Solomon et al., which obtained activation barriers of 80, 69, and 68 kJ/mol, respectively.[14,15,18−20,23,24] According to the generally accepted mechanism, the reaction starts by DMSO entering the active site via a first transition state, leading to an intermediate with DMSO weakly bound to the Mo^{IV} center. In the second step, the S−O bond is cleaved in an OAT reaction[17,19] coupled with a two-electron transfer. All previous investigations have found that the second transition state is rate-limiting with a barrier of 38−80 kJ/mol.[12−15,17−19,23,24] We have shown that the calculated barriers strongly depend on details of the theoretical method and that a proper account of dispersion and solvation effects is needed, together with large basis sets and accurate density functional theory (DFT) methods.[20]

SO is a vital enzyme, responsible for the oxidation of sulfite to sulfate. Three distinct mechanisms have been proposed for SO and its functional inorganic models.[8,9,25] In one mechanism, the lone-pair electrons of the substrate sulfur atom attack the equatorial oxo ligand of Mo, leading to the formation of a S−O bond (S → OMo mechanism). Alternatively, it has been suggested that the sulfide substrate coordinates first to the Mo ion, either through the sulfur atom (S → Mo mechanism) or by one of the oxygen atoms (O → Mo mechanism).[26] Thapper and co-workers have compared the S → OMo and S → Mo mechanisms and concluded that the former was more likely.[9] Hernandez-Martin and Ziegler also argued for this mechanism.[27] On the other hand, Sarkar and co-workers compared the S → OMo and O → Mo mechanisms, and argued that the latter is preferable,[28] based on molecular orbitals, atomic charges, and the fact that only this mechanism can give rise to saturation kinetics that has been observed both for the enzyme reaction and functional inorganic models.[8,29] We have recently studied all three mechanisms with the same methods, using both HSO_3^- and SO_3^{2-} as the substrate. The results show that the S → OMo mechanism has a lower activation barrier than the other mechanisms.

XO catalyzes the oxidation of hypoxanthine to xanthine and also the oxidation of xanthine to uric acid. It plays an important role in the catabolism of purines.[16,30] Extensive experimental and theoretical investigations have been performed on XO and related enzymes.[3,7,31−37,65] The results indicate that the XO reaction proceeds via a proton transfer from the Mo^{VI}−OH group to a conserved Glu residue, followed by nucleophilic attack of the resulting Mo^{VI}=O group on the substrate and a hydride transfer from the substrate to the Mo=S ligand. Page et al. proposed a radical mechanism, in which two sequential one-electron transfers give rise to a small overall activation barrier.[38] However, Hille and co-workers demonstrated that XO most likely operates via a two-electron mechanism with formation of a Mo^{IV} intermediate, followed by hydride transfer to the Mo center.[39] In a recent combined QM and molecular mechanics (QM/MM) study of XO,[36] Thiel et al. demonstrated that the latter mechanism is favorable and that the hydride transfer is slowest among the modeled chemical steps (the product release is rate limiting for the net reaction).[40] This has also been confirmed by a subsequent study considering the effects of variations in the cofactor, the substrate, and an active-site Glu residue on the reaction mechanism.[37]

In this paper, we want to understand why the Mo coordination sphere of the three Mo oxo-transfer enzyme families is different (i.e., why the three families employ the different sets of Mo ligands shown in Scheme 1) and whether these differences play a functional role. Such questions are hard to answer with experimental methods, because the primary sequence of the various enzymes is very different. However, with quantum mechanical (QM) methods this is feasible, because we can study models with the Mo ion and its first-sphere ligands. They show the intrinsic reactivity of the metal ion with a certain set of ligands. This is supported by previous computational studies that have shown that the native reactions of DMOSR, SO, and XO can be satisfactorily studied by cluster models of the active site.[8−38] By changing the ligands in these models, we can compare the intrinsic reactivity of the various ligands set. Thereby, we can study both thermodynamic (reaction energies, redox potentials, etc.) and kinetic factors (activation barriers). The results contribute to our understanding of the design of the Mo OAT enzyme families.

2. METHODS

2.1. Model Systems Setup. The starting coordinates for the various computational models were derived by truncation of available crystal structures of relevant enzymes,[41−43] in accordance with previous computational work.[19,27,36] To reduce the computational load, the MPT ligand was modeled by 1,2-dimethyldithiolene ($[(MeCS)_2]^{2-}$; DMDT), which also has been used in many of the previous studies.[12,17,19,20,23,24,26,28,33] The protein-derived cysteine and serine ligands were modeled by MeS^- and MeO^-, respectively, whereas other groups were not truncated. Consequently, the oxidized

dx.doi.org/10.1021/ic5010837 | Inorg. Chem. 2014, 53, 11913−11924

active sites of DMSOR and SO were represented by $[MoO(MeO)(DMDT)_2]^-$ and $[MoO_2(MeS)(DMDT)]^-$, whereas the XO active site was modeled either by the protonated $[MoOS(DMDT)(OH)]^-$ model or by the deprotonated $[MoO_2S(DMDT)]^{2-}$ model, i.e., before or after the initial proton transfer to the active-site Glu residue (the two models will be called XOH and XO in the following). All these models are shown in Scheme 2.

Scheme 2. Model Systems Used in the Calculations[a]

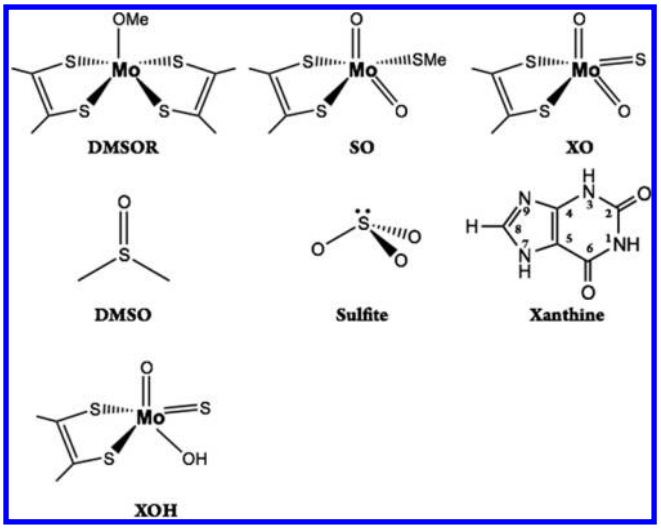

[a]The upper row shows the three active-site models in their oxidized states: left, DMSOR; middle, SO; and right, deprotonated XO. The middle row shows the corresponding native substrates: left, DMSO; middle, SO_3^{2-}; and right, neutral xanthine. The bottom row shows the protonated XO model.

To study the thermodynamics properties of the models, we used ten models of the type $MoO(DMDT)XY$, where X = $DMDT^{2-}$, O^{2-}, or S^{2-}, and Y = OMe^-, SMe^-, OH^-, or O^{2-}. Thus, X = $DMDT^{2-}$, Y = OMe^- gives our standard DMSOR model, X = O^{2-}, Y = SMe^- is our SO model, and X = S^{2-}, Y = OH^- and O^{2-} are our XO models before and after the initial proton-transfer step, whereas the other systems are intermediate mixed models.

For the xanthine substrate, the protonation state is crucial. The most stable neutral tautomer of xanthine is protonated on the N_1, N_3, and N_7 atoms (shown in Scheme 2). However, according to the QM/MM studies,[30,36] this state is deprotonated on the N_3 atom by an active-site Glu residue (and because the Glu residue is not included in our calculations, we start our reaction from this deprotonated state) and then accepts a proton from Mo-bound OH^- group, giving a neutral xanthine, protonated on the N_1, N_7, and N_9 atoms.

2.2. QM Calculations. All QM calculations were performed with the ORCA software,[44] using the hybrid B3LYP density functional.[45,46] B3LYP is the most widely used density functional, and it has a well documented accuracy: For molecules containing first- and second-row atoms, the errors are seldom higher than 13 kJ/mol, and for transition-metal biochemistry, the accuracy is normally within 21 kJ/mol.[47] In previous studies of the DMSOR reaction, B3LYP gave the best activation barrier compared to LCCSD(T) calculations[20] and it was deemed to be the most accurate functional among a set of 17 DFT methods by comparison to CCSD benchmark values.[24] It has also been employed in most of the previous studies.[3,12,14,15,17,19,23] However, to get a feeling of the stability of the results, all energies were also calculated by single-point energy calculations with the pure TPSS functional.[48] The results of these calculations are presented in Tables S1–S6 in the Supporting Information (keeping the basis sets and all the corrections the same as for the B3LYP calculations). They often show significant changes in the absolute energies, especially for reactions involving a change in the oxidation state of Mo (up to 60 kJ/mol). However, the energy differences are more stable (i.e., trends) and none of the general conclusions of the paper change with this variation of the DFT functional.

The def2-TZVPP basis set[49] was employed for all elements throughout the study. The density-fitting and chain-of-sphere technique, also called resolution-of-the-identity approximation RIJ-COSX,[50] was employed with the auxiliary basis set def2-TZVP/J to accelerate the calculations at insignificant loss in accuracy. Test calculations for the DMSOR reaction were also performed with the larger def2-QZVPP basis set, showing that the energies were converged to within 9 kJ/mol.

Relativistic corrections were found to be non-negligible for geometries and energies. Therefore, all calculations were performed using the zeroth-order regular approximation (ZORA)[51] to include scalar relativistic effects. These calculations used the ZORA-adapted segmented all-electron relativistically contracted (SARC) version of the def2-TZVPP basis sets for all atoms.

The DFT-D2 dispersion correction was applied to all B3LYP calculations (also the geometry optimizations).[52] To take into account the role of polar solvent effect, the conductor-like screening model (COSMO)[53] with a dielectric constant of 4 and optimized radii for H, C, N, O, and S[54] (1.30, 2.00, 1.83, 1.72, and 2.16 Å; 2.22 Å for Mo) was used for all calculations to mimic the protein surroundings. In addition, nonpolar continuum-solvation cavitation, dispersion, and repulsion energies were estimated for all complexes with the polarized continuum method (PCM)[55−57] as implemented in Gaussian 03.[58] These calculations used the UAKS radii (united atom topological model for Kohn−Sham theory),[56] and they are needed to obtain valid solvation energies for all reactants, as well as a balance in the dispersion energy terms for reactions in which a ligand from solution binds to or dissociates from a metal complex.[59]

The geometries were fully optimized without symmetry constraints using an unrestricted open-shell formalism. In all calculations, the convergence criteria were set to tight SCF convergence and finer-than-default integration grids (Grid4 in ORCA convention) in order to get fully converged stationary points with accurate energies on the minimum-energy pathways. Harmonic vibrational frequencies were computed to verify the nature of the stationary points. The minimum structures reported in this paper possess only positive eigenvalues of the Hessian matrix, whereas the transition states have a single negative eigenvalue. Zero-point energies (ZPE), entropy, and thermal corrections to the enthalpy for the optimized geometries were obtained from the frequency calculations using an ideal-gas rigid-rotor harmonic-oscillator approximation at 300 K and 1 atm pressure.

In summary, geometries were optimized at the B3LYP-D2/def2-TZVPP+ZORA+COSMO level and energies were corrected by PCM nonpolar solvation energies, ZPE, and thermal corrections.

The studied Mo complexes have several potentially accessible spin states. Most previous studies have concentrated on the low-spin closed-shell singlet states, but it has been discussed whether the triplet state may also be accessible.[17] Therefore, we have also explored the triplet state for the native reactions. However, the results indicate that the triplet state is energetically unfavorable for all states in all reactions. Furthermore, broken-symmetry calculations were also performed for the open-shell singlet state of the transition states, but no wave functions with significant spin polarization were found. We therefore discuss only the singlet-state surfaces in the following.

2.3. Reduction Potentials and Acidity Constants. Absolute reduction potentials were calculated from the free energy difference between the oxidized and reduced states, corrected to the scale of the normal hydrogen electrode by adding 4.28 V.[60] The translational free energy of a free electron (0.03 kJ/mol) was ignored.

$$E_0 = E_{ox} - E_{red} - 4.28 \quad (1)$$

Likewise, absolute pK_a values were calculated from the free energy difference between the deprotonated and protonated states, corrected by a factor of −1131.0 kJ/mol, which represents the sum of the estimated hydration free energy of a proton, the translational Gibbs free energy of a proton at 300 K and 1 atm, and the change in reference state from 1 atm to 1 M at 300 K.[60,61]

dx.doi.org/10.1021/ic5010837 | Inorg. Chem. 2014, 53, 11913−11924

3. RESULTS AND DISCUSSION

In this paper, we compare the intrinsic reactivities of active-site cluster models of the three families of Mo OAT enzymes with DFT methods. We will in separate sections compare thermodynamic (reaction free energies, redox potentials, acidity constants, and water-binding energies) and kinetic (enzyme mechanism and activation barriers) of these models.

As shown in Schemes 1 and 2, the active sites of the three families of mononuclear Mo enzymes (DMOSR, SO, and XO) can in their oxidized state be modeled by $[MoO(MeO)(DMDT)_2]^-$, $[MoO_2(MeS)(DMDT)]^-$, and $[MoOS(OH)(DMDT)]^-$. Thus, all three enzymes have four ligands, including one DMDT group and one oxo atom (which is transferred to the substrate). It is the other two ligands that differ, and we will call these ligands X and Y in the following, so that the DMSOR family has X = $DMDT^{2-}$ and Y = MeO^-, the SO family has X = O^{2-} and Y = MeS^-, and the XO family has X = S^{2-} and Y = OH^-. Note that the X ligand always has a double negative charge and the Y ligand a single negative charge. However, as mentioned in the Introduction, the first step of the XO reaction is a proton transfer from the OH^- ligand to an active-site Glu residue, so that the actual reactive species of XO in the subsequent reactions actually has Y = O^{2-}. Therefore, we included also this group in the investigation. Our aim is to understand why the families have selected these differing sets of ligands.

3.1. Thermodynamics. *3.1.1. Reaction Free Energies.* We first explored the reaction free energies, i.e., the thermodynamic driving force for the general OAT reaction,

$$Mo^{VI}O(DMDT)XY + Z \rightarrow Mo^{IV}(DMDT)XY + ZO \quad (2)$$

where Z represents one of the three substrates of the three enzymes (i.e., DMS, SO_3^{2-}, or Xan). The calculated reaction free energies of the native sets of ligands, as well as mixtures of X and Y ligands, are listed in Table 1.

Table 1. Reaction Free Energies (kJ/mol) of the General OAT Reaction in Eq 2

		free energy (kJ/mol)		
X	Y	DMS[a]	SO_3^{2-}[a]	Xan[a]
DMDT	OMe	63.3	−137.4	−41.1
DMDT	SMe	75.6	−125.1	−28.8
DMDT	OH	60.9	−139.8	−43.4
O	OMe	151.6	−49.1	47.3
O	SMe	150.2	−50.5	45.9
O	OH	150.7	−50.0	46.3
S	OMe	159.7	−41.0	55.3
S	SMe	164.3	−36.4	60.0
S	OH	155.5	−45.2	51.1
S	O	149.2	−51.5	44.8

[a]Z in eq 2.

It can be seen that the oxidation of DMS to DMSO is endergonic for all combinations of ligands X and Y (by 61−164 kJ/mol; 63 kJ/mol for the native DMSOR model), indicating that the actual reaction (reduction of DMSO) is exergonic for all models. Likewise, the oxidation of sulfite to sulfate is exergonic for all combinations of ligands (by −36 to −140 kJ/mol; −50 kJ/mol for the native SO model). On the other hand, the oxidation of Xan is in endergonic for the native XOH model by 51 kJ/mol. However, this estimate critically depends on the protonation states of the models and the surroundings. In Table 1, we assume that Xan is its most stable protonation state (neutral and protonated on the N_1, N_3, and N_7 atoms) and that uric acid is also neutral, although it is singly deprotonated in neutral aqueous solution (the pK_a is 5.4). In fact, in the thorough QM/MM study of XO, Metz and Thiel started from the XOH model and the most stable tautomer of Xan and ended up with a protonated SH group, singly deprotonated urate, and a protonated conserved Glu residue with a favorable reaction energy of −38 kJ/mol, indicating that the enzyme reaction actually is exothermic.[36] However, they did not model the binding of the substrate, the dissociation of the product, or regeneration of the deprotonated Glu residue, so the results are not fully comparable with ours.

Thus, the thermodynamic driving force of the OAT reaction does not give any clear clue why the different active sites are used. However, the energies in Table 1 show some interesting trends. First, we note that the energies were obtained for isolated active-site models and substrates or products. Therefore, the *relative* energies for different sets of X and Y ligands are independent of the substrate. In fact, the three columns in Table 1 are simply translated by a constant offset, which is (using Z = DMS as the reference) −201 and −104 kJ/mol for SO_3^{2-} and Xan, respectively. Therefore, we can insert also the substrate/product pairs together with the active-site models on a common energy scale of oxygen atom affinity. This is analogous to the thermodynamic oxo-transfer reactivity scale suggested by Holm, and our results are in agreement those results, e.g., for the relative positions of the SO_3^{2-}/SO_4^{2-} and DMS/DMSO pairs.[62−64] Continuing to use the DMS/DMSO pair as the reference (i.e., the DMS/DMSO pair gets an energy of 0 kJ/mol and all the enzyme models attain the energies of the DMS column in Table 1), the SO_3^{2-}/SO_4^{2-} gets an energy of 201 kJ/mol, i.e., larger than any of the enzyme models, in accordance with the above observation that all models could catalyze the oxidation of sulfite. The Xan substrate gets an energy of 104 kJ/mol, showing that it can only be oxidized by the three enzyme models involving X = DMDT.

Moreover, we see that all models with X = DMDT give more negative energies than the other two X ligands (by 74−103 kJ/mol). Thus, it is clear that the DMSOR active site has an appreciably higher oxidizing power than the active sites of the other two enzyme families, in spite of the fact that DMSOR catalyzes the reduction of DMSO. This indicates that the ligands of DMSOR were chosen not to maximize the reaction free energy but rather to keep it negative, but as close to zero as possible to save energy.

The driving forces for the three singly charged Y ligands are quite similar, and the order depends on the X ligand (the variation is 5−9 kJ/mol for X = O^{2-} or S^{2-} and 15 kJ/mol for X = $DMDT^{2-}$). The Y = O^{2-} ligand gives 6−15 kJ/mol more negative energies than the singly charged ligands, showing that the reducing power of the enzyme models increases if the OH^- ligand is deprotonated, as is believed to take place in the XO reaction.[36,65] Consequently, the DMSOR has the most oxidizing active site by 74−103 kJ/mol, whereas the XO site with a OH^- ligand is 5 kJ/mol more reducing than the SO site, although this is inverted to −1 kJ/mol if the OH^- ligand is deprotonated.

3.1.2. Redox Potentials and Acidity Constants. Once the OAT reaction is completed, the active site needs to be either rereduced (DMSO) or reoxidized (SO and XO) by two

dx.doi.org/10.1021/ic5010837 | Inorg. Chem. 2014, 53, 11913−11924

stepwise one-electron-transfer reactions, coupled by the conversion of an oxy group to a water ligand by the binding of two protons (DMSOR) or vice versa. These reactions are governed by a series of reduction potentials (E_0) and acidity constants (pK_a values) as is illustrated in Scheme 3. The calculated values of these parameters for the various models are given in Tables 2−4.

Scheme 3. Electron- and Proton-Transfer Reactions Needed To Interconvert the Reduced and Oxidized States of the Various Enzyme Active Sites

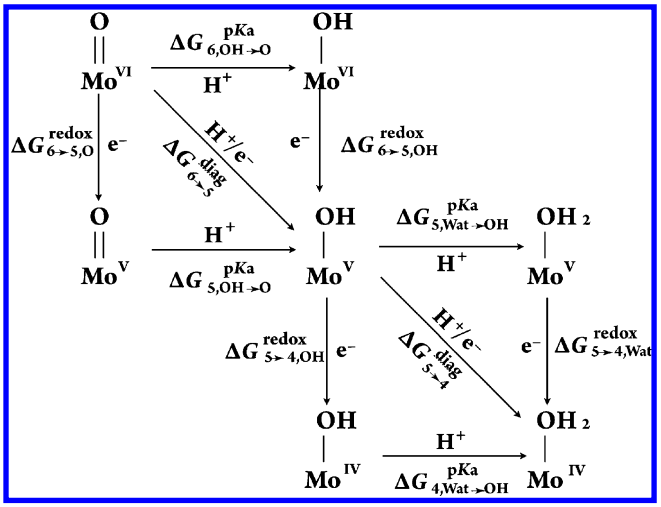

Table 2. The Four Reduction Potentials (V) in Scheme 3 for the Ten Models

X	Y	$\Delta G^{redox}_{6\to5,O}$	$\Delta G^{redox}_{6\to5,OH}$	$\Delta G^{redox}_{5\to4,OH}$	$\Delta G^{redox}_{5\to4,Wat}$
DMDT	OMe	−2.70	−0.66	−2.92	−0.24
DMDT	SMe	−2.46	−0.43	−2.77	−0.49
DMDT	OH	−2.38	−0.55	−2.89	−0.25
O	OMe	−3.14	−0.55	−3.38	−1.15
O	SMe	−2.85	−0.23	−3.01	−0.93
O	OH	−3.19	−0.21	−3.31	−1.11
S	OMe	−2.72	−1.19	−3.40	−1.13
S	SMe	−2.42	−0.97	−3.36	−1.01
S	OH	−2.72	−0.85	−3.38	−1.15
S	O	−4.97	−2.71	−5.45	−2.41

Table 3. The Four Acidity Constants (pK_a Units) in Scheme 3 for the Ten Models

X	Y	$\Delta G^{pK_a}_{6,OH\to O}$	$\Delta G^{pK_a}_{5,OH\to O}$	$\Delta G^{pK_a}_{5,Wat\to OH}$	$\Delta G^{pK_a}_{4,Wat\to OH}$
DMDT	OMe	10.6	45.2	16.0	61.1
DMDT	SMe	8.3	42.6	12.8	51.3
DMDT	OH	11.7	42.7	13.6	58.1
O	OMe	10.8	54.7	11.1	48.7
O	SMe	8.8	53.2	7.9	43.0
O	OH	6.5	56.8	10.0	47.3
S	OMe	9.9	35.8	21.5	59.8
S	SMe	7.8	32.4	18.9	58.5
S	OH	4.8	36.4	20.8	58.6
S	O	43.8	82.1	40.6	92.1

It can be seen that all reduction potentials are negative (−0.2 to −5.5 V). Y = O^{2-} always gives a much more negative potential than the singly charged Y ligands, showing that the extra negative charge stabilizes the oxidized state. Likewise, the reduction potential going from the Mo(VI) to the Mo(V) state is ∼2 V more negative with an oxy group ($\Delta G^{redox}_{6\to5,O}$) than with a OH^- ligand ($\Delta G^{redox}_{6\to5,OH}$). $\Delta G^{redox}_{6\to5,O}$ is most negative for X = O^{2-}, whereas DMDT and S^{2-} have similar potentials. Y = MeS^- gives more positive potentials than the other two Y ligands. For $\Delta G^{redox}_{6\to5,OH}$, X = S^{2-} gives the most negative potentials and Y = MeS^- gives the most positive potentials.

Table 4. Reaction Energies of the Two Hydrogen Atom Transfer Reactions in Scheme 3 (Diagonal Reactions; V) for the Ten Models

X	Y	$\Delta G^{diag}_{6\to5}$	$\Delta G^{diag}_{5\to4}$
DMDT	OMe	−0.03	0.70
DMDT	SMe	0.05	0.27
DMDT	OH	0.15	0.55
O	OMe	0.09	−0.50
O	SMe	0.29	−0.46
O	OH	0.18	−0.51
S	OMe	−0.60	0.14
S	SMe	−0.51	0.11
S	OH	−0.57	0.08
S	O	−0.11	−0.01

The results are similar for the Mo(V) → Mo(IV) potentials: They are 2−3 V more negative with an OH^- ligand ($\Delta G^{redox}_{5\to4,OH}$) than with a water ligand ($\Delta G^{redox}_{5\to4,Wat}$). Both $\Delta G^{redox}_{5\to4,OH}$ and $\Delta G^{redox}_{5\to4,Wat}$ are least negative for X = DMDT. For $\Delta G^{redox}_{5\to4,OH}$, the singly charged Y ligands give the trend $MeO^- < OH^- < MeS^-$.

The calculated pK_a values in Table 3 show similar trends: All pK_a values are positive, and only two of them are lower than 7, indicating that protonation is predicted to be favorable for almost all complexes in water solution (but note that the calculations were performed in a continuum solvent with a dielectric constant of 4, i.e., lower than that of water, 80). The pK_a values are much higher (by 24−51 pK_a units) for the reduced complexes than for the oxidized ones, as expected, showing that the reduced complexes always are expected to be protonated. Y = O^{2-} always gives much larger pK_a values than the singly charged Y ligand (by 20−46 pK_a units).

$\Delta G^{pK_a}_{6,OH\to O}$ shows only small variations with the ligands, and the only consistent trends are that it is higher for X = O^{2-} than S^{2-} and lower for Y = MeS^- than MeO^-. $\Delta G^{pK_a}_{5,OH\to O}$ shows a much larger variation, with the X trend S^{2-} < DMDT < O^{2-}. $\Delta G^{pK_a}_{5,Wat\to OH}$ shows the opposite X trend, whereas $\Delta G^{pK_a}_{4,Wat\to OH}$ is smallest for X = O^{2-}. The Y trend is $MeO^- > OH^- > MeS^-$.

Table 4 lists the calculated energies for the diagonal hydrogen atom transfer reactions in Scheme 3. The results are given in V to emphasize that they depend on electrons and protons from external sources (like the reduction potentials and acidity constants in Tables 2 and 3). It can be seen that they are all rather close to zero (−0.6 to 0.7 V). $\Delta G^{diag}_{6\to5}$ for the Mo(VI) → Mo(V) transition is more negative for X = DMDT and S^{2-} than for O^{2-}. Y = O^{2-} gives a much less negative result than the singly charged Y ligands. $\Delta G^{diag}_{5\to4}$ follows the X trend O^{2-} < S^{2-} < DMDT, whereas the Y trend is varying. Consequently, the XO models have more negative $\Delta G^{diag}_{6\to5}$ (−0.6 or −0.1 V) than the other two native enzyme models (0.0 and 0.3 V). On the other hand SO has a more negative $\Delta G^{diag}_{5\to4}$ (−0.5 V) than the other two enzyme models (0.7 and 0.0−0.1 V). For the full proton-coupled Mo(VI) → Mo(IV) reduction ($\Delta G^{diag}_{6\to5}$ + $\Delta G^{diag}_{5\to4}$), the SO and XO models have negative potentials (−0.2 and −0.1 or −0.5 V, indicating that the oxidized state is more

dx.doi.org/10.1021/ic5010837 | Inorg. Chem. 2014, 53, 11913−11924

stable), whereas the DMSOR model has a positive potential (0.7 V, i.e., the reduced Mo^{IV} state is most stable). Interestingly, this is in accordance with the starting states for the OAT reactions of the three enzymes, indicating that the active sites have been constructed to make the reoxidation or rereduction reactions favorable.

3.1.3. Water-Binding Free Energies. In the general OAT reaction, an oxy group is transferred from the Mo(VI) active site to the substrate, giving a Mo(IV) ion with one ligand less than in the oxidized state. In many enzymes, this decrease in the coordination number is compensated by the binding of a water molecule. Therefore, we have calculated the binding energy of a water molecule to the reduced active-site models, i.e., the energy of the reaction

$$Mo^{IV}(DMDT)XY + H_2O \rightarrow Mo^{IV}(DMDT)(H_2O)XY \quad (3)$$

The results of these calculations are collected in Table 5. It can be seen that all binding free energies are positive (2−33 kJ/mol), indicating that the binding of water is unfavorable. This is caused by the unfavorable loss of translational and rotational entropy of the bound water molecule. It has been argued that the simple Sackur−Tetrode equation, used in these estimates, overestimate this contribution in water solution by ∼30 kJ/mol.[66−68] This makes the absolute values of the energies uncertain, but the relative values should be more reliable.

Table 5. Gibbs Free Energies (kJ/mol) for the Water-Binding Reaction in Eq 3

X	Y	ΔG
DMDT	OMe	9.5
DMDT	SMe	32.6
DMDT	OH	15.8
O	OMe	19.0
O	SMe	3.3
O	OH	15.4
S	OMe	13.3
S	SMe	8.9
S	OH	21.7
S	O	2.2

Unfortunately, the trends are quite varying. The most conspicuous effect is that the results with Y = MeS^- always differ from the other results. However, for X = DMDT, Y = MeS^- gives a weaker binding than the other two ligands (by 17−23 kJ/mol), whereas for the other two X ligands, it instead gives a stronger binding (by 4−16 kJ/mol; Y = O^{2-} gives an even stronger binding). As a result, the three native models all give small energies (2−9 kJ/mol; in the reduced state, the XO model with Y = O^{2-} is the relevant one, as we will see below).

To sum up, we have seen that the DMDT ligand gives the strongest oxidative power. The ligands seem to have been chosen not to give as exergonic an OAT reaction as possible, but instead to keep the energy loss as low as possible. In fact, the active sites seem to have been designed to make the rereduction (DMSOR) or the reoxidation (SO and XO) of the enzyme possible.

3.2. Kinetics. In the previous section, we studied thermodynamic differences between active site models with different ligands, related to those found in the three families of Mo OAT proteins. In this section, we instead turn to kinetic effects and study mechanisms and activation energies for the catalysis of three typical OAT reactions, viz., DMSO → DMS, SO_3^{2-} → SO_4^{2-}, and Xan → uric acid (Scheme 4).

Scheme 4. OAT reactions considered for the three substrates, DMSO (left), sulfite (middle), and xanthine (right)

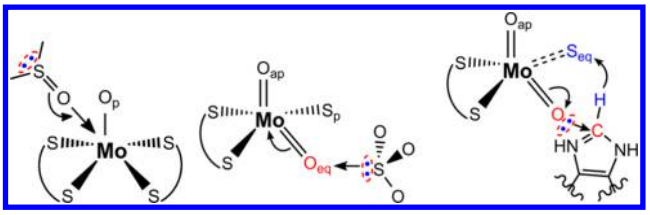

Optimizations of transition states are more demanding than equilibrium states. Therefore, we have restricted this part of the investigation to active-site models of the native enzymes, i.e. (in the oxidized state), $[MoO(DMDT)_2(MeO)]^-$ (DMSOR), $[MoO_2(DMDT)(MeS)]^-$ (SO), and $[MoO_2S(DMDT)]^-$ (XO). Thus, we have studied the nine combinations of three reactions and three active-site models. The various calculations will be denoted by the abbreviation for the enzyme (i.e., the active-site model DMSOR, SO, or XO) and the substrate (DMSO, SO_3^{2-}, or Xan), e.g., the SO−DMSO reaction.

3.2.1. The DMSOR−DMSO Reaction. We start with the native DMSOR−DMSO reaction, in which DMSO is converted to DMS. This reaction has been the subject of several previous theoretical studies.[8,12,14,17−20,22,24] In accordance with these, we find in addition to the separated reactants (SR) and separated products (SP) an intermediate (IM) in which DMSO is coordinated to Mo(IV) by the oxygen atom. These three states are connected by two transition states, the first for the formation of the Mo−O bond (TS1) and the second for the cleavage of the S−O bond of the substrate (TS2). The structures of these five stationary points are shown in Figure 1. The structures closely resemble those found in previous studies (geometric parameters are shown in Table S7 in the Supporting Information),[8,9,14,15,17−19,22,24] so they will not be further discussed. In particular, we find a major change in the structure

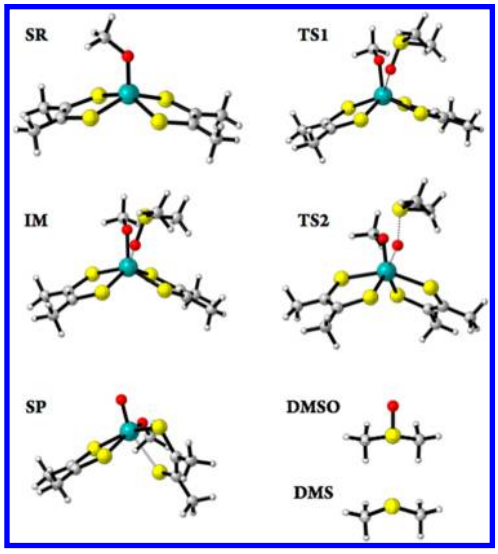

Figure 1. Structures of the various states along the DMSOR−DMSO reaction obtained at the B3LYP-D2/def2-TZVPP+ZORA+COSMO level.

dx.doi.org/10.1021/ic5010837 | Inorg. Chem. 2014, 53, 11913−11924

Table 6. Relative Enthalpies (kJ/mol) along the Reaction Paths for the Studied Reactions

state	DMSOR−DMSO	SO−DMSO	XO−DMSO	XOH−DMSO	SO−SO_3^{2-}	DMSOR−SO_3^{2-}	XO−SO_3^{2-}	XOH−SO_3^{2-}	XO−Xan	XO_3[b]−Xan
SR	0.0	0.0	0.0	0.0	0.0	0.0	0.0	0.0	0.0[a]	0.0[c]
TS1	28.1	−0.1	36.4	−42.2	167.1	177.1	454.7	182.9	61.9	78.2
IM	28.6	−45.5	31.7	−187.4	16.1	41.1		63.8	51.2	56.0
TS2	83.2	−12.3	39.7	−34.9	120.0	28.4		116.0	68.0	128.3
SP	−62.5	−150.5	−148.2	−156.1	−49.3	−137.3	−51.6	−53.4	−52.5	−9.4

[a]preR (with XOH); RC is at 24.4 kJ/mol. [b]XO_3 = $[MoO_3(DMDT)]^{2-}$. [c]preR; RC is at 14.4 kJ/mol.

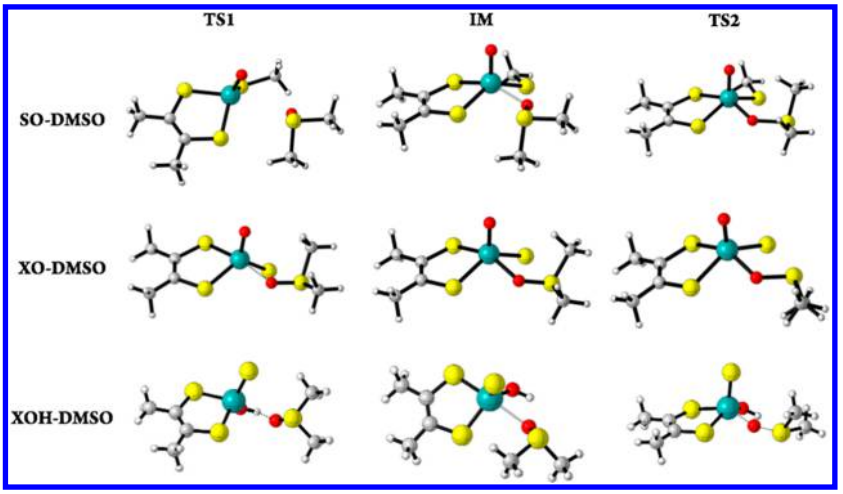

Figure 2. Structures of the TS1, IM, and TS2 states along the SO−DMSO, XO−DMSO, and XOH−DMSO reactions obtained at the B3LYP-D2/def2-TZVPP+ZORA+COSMO level.

of the product complex to octahedral, which is incompatible with trigonal prismatic structure of the enzyme active site.[2−4,10] However, this change in geometry is not expected to affect the activation energies significantly, because neither of the two transition states shows an octahedral structure.

The corresponding reaction enthalpies are collected in Table 6. It can be seen that IM is 29 kJ/mol less stable than SR. TS1 is very close in energy to IM: with all energy corrections it is actually within 1 kJ/mol of IM. The highest energy on the potential-energy surface is that of TS2, which is 83 kJ/mol above SR. The reaction energy is −63 kJ/mol. As discussed before,[20] the energies are very sensitive to the size of the basis sets and the DFT functional, with sizable dispersion corrections. The calculated barrier is somewhat too large, compared to experiments, 62 kJ/mol.[10,69] The reason for this is partly the DFT functional, partly the omission of the surrounding enzyme. Calibration calculations with the local CCSD(T0) method have shown that energies calculated with the current methodology have errors of 19−45 kJ/mol for the reaction mechanism of DMSOR.[20] This has to be kept in mind when considering the current results. Fortunately, the smallest error was observed for the rate-limiting barrier (of TS2), which is the most important energy in the present comparison of the various enzyme models.

3.2.2. The SO−DMSO Reaction. Next, we study whether the SO model ($[MoO(DMDT)(MeS)]^-$) may catalyze DMSO reduction. We obtained the same five states, SR, TS1, IM, TS2, and SP, as those for the native DMSOR reaction. The geometry of IM is quite similar for the SO and DMSOR models (Figure 2), but the Mo−O_{DMSO} bond is somewhat shorter in the former, 2.24 Å, compared to 2.31 Å (the geometric parameters are listed in Table S8 in the Supporting Information). However, TS1 is much earlier for the SO model with a Mo−O_{DMSO} distance of 3.20 Å, compared to 2.62 Å in the DMSOR model. On the other hand, the geometries of TS2 are quite similar with differences of only 0.04−0.05 Å in the forming Mo−O_{DMSO} bond and the breaking S−O_{DMSO} bond.

From the results in Table 6, it can be seen that the energies are quite different for the two models: The first activation energy (TS1) is appreciably lower for the SO model, 0 kJ/mol, compared to 28 kJ/mol for the DMOSR model. Moreover, the IM intermediate is much more stable; it is actually 46 kJ/mol more stable than SR (29 kJ/mol less stable for the DMOSR model). The second activation barrier is also appreciably lower for the SO model, 33 kJ/mol relative IM, compared to 55 kJ/mol for the DMSOR model. Finally, the products are 88 kJ/mol more stable for the SO model than for the DMSOR model. It is this large difference in the driving force of the reaction energy (already discussed in section 3.1.1) that lowers the energies of all states in the reaction (relative to RS). All together this demonstrates that the isolated SO active site is predicted to readily catalyze the DMSO reduction to DMS, actually with a lower barrier than the native active site.

3.2.3. The XO−DMSO Reaction. Next, we study the DMSO reaction with the XO model. We first consider the deprotonated $[MoO_2S(DMDT)]^{2-}$ model (XO). Also with this model, we can obtain all five states of the reaction. From Figure 2 and Table S9 in the Supporting Information, it can be seen that IM is quite different from what was obtained with the DMSOR and SO models, with a Mo−O_{DMSO} distance of only 2.10 Å (2.31 and 2.24 Å for the other two models) and an elongated O−S_{DMSO} bond length of 1.62 Å (1.53 and 1.54 Å for the other two models). TS1 also has a much shorter Mo−O_{DMSO} distance (2.35 Å) than in the other two models (2.62 and 3.20 Å). In TS2, the differences are smaller, but the breaking O−S_{DMSO} bond is 0.10−0.15 Å shorter than for the

dx.doi.org/10.1021/ic5010837 | Inorg. Chem. 2014, 53, 11913−11924

other two complexes and the forming Mo−O_{DMSO} bond is 0.06−0.10 Å longer.

The energies of the DMSO reaction with the XO model are more similar to those of the native DMSOR model than to those of the SO model. The energy of IM for the XO and DMSOR models is nearly the same, 32 and 29 kJ/mol. Likewise, the energy of TS1 is similar to that of IM, 36 kJ/mol for the XO model. On the other hand, the reaction energy is much more negative for the XO model (−148 kJ/mol) than for the DMSOR model (−63 kJ/mol); it is actually similar to what was found for the SO model (−151 kJ/mol). Consequently, the second activation barrier is much lower for the XO model than for the DMSOR model (40 compared to 83 kJ/mol), which is only 3 kJ/mol higher than the barrier of TS1. This indicates that the XO model can also catalyze the OAT of DMSO to DMS with a rate that is actually higher than that of the native DMSOR model.

With the XOH model ([MoOS(OH)(DMDT)]$^-$), IM is strongly stabilized and SP is somewhat more stable than for the XO model (187 and 156 kJ/mol more stable than SR, respectively). On the other hand, TS2 is 152 kJ/mol above IM, giving a prohibitively large barrier (owing to the over-stabilization of IM). This reaction also ends up in a state with sulfido ligand in the apical position, rather than the oxo group, as in the protein, but such a structure is only 2 kJ/mol less stable than the protein conformation.

3.2.4. The SO–SO_3^{2-} Reaction. Next, we turn to the oxidation of SO_3^{2-} and consider how it is catalyzed by the SO model. For this reaction, three different mechanisms have been suggested,[8,26,70] but recent calculations indicate that the most probable one involves an attack of the substrate S atom on the equatorial oxy group of the active-site Mo. Such a mechanism is essentially the reverse of the DMSOR reaction: It starts from the SO model with two oxy groups and the metal in the Mo(VI) state. The substrate approaches the equatorial oxy group by the S atom, leading to the formation of a S−O bond and therefore a Mo(IV)−OSO_3 intermediate, IM, via a first transition state (TS1). In TS1, the S−O distance between SO_3^{2-} and the equatorial oxo group is 2.51 Å, and the Mo−O_{eq} bond length is 1.78 Å, indicating a rather early transition state. Next, SO_4^{2-} dissociates via a second transition state TS2. Structures of the five states are shown in Figure 3. The corresponding bond lengths are listed in Table S10 in the Supporting Information, and they are similar to what has been found previously,[9,27,28] so they will not be discussed in detail.

The relative enthalpies of the SO–SO_3^{2-} reaction are collected in Table 6. It can be seen that the highest barrier is found for TS1, 167 kJ/mol. The intermediate IM is 16 kJ/mol above SR. The second transition state, TS2, is lower than TS1, 120 kJ/mol above SR and 104 kJ/mol above IM. SP is 49 kJ/mol more stable than SR.

Clearly, the estimated activation energy is too high for an enzyme reaction: the experimental barrier is 52 kJ/mol.[27,29] The high barrier is mainly caused by the electrostatic repulsion between the Mo active site and the substrate, which both are negatively charged. It depends strongly on the dielectric constant used for the continuum-solvation model in the calculations, the DFT functional, and the basis sets. In our previous calculations with LCCSD(T0) energies and a dielectric constant of 80, the barrier was 60 kJ/mol lower.[27] However, since we are mainly interested in the relative energies for the various enzyme models, we have decided to discuss results that are consistent with all the other calculations (i.e., with a dielectric constant of 4), even if they give a too high barrier.

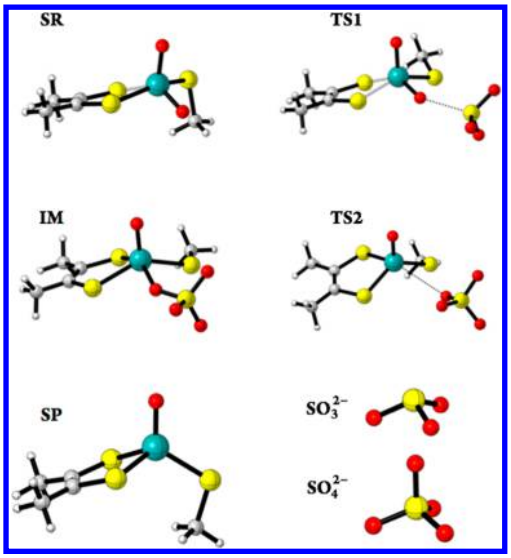

Figure 3. Structures of the various states along the SO–SO_3^{2-} reaction obtained at the B3LYP-D2/def2-TZVPP+ZORA+COSMO level.

Previous QM-cluster studies have obtained similar high barriers,[9,25,27] unless the active site has been neutralized by the addition of a positively charged residue.[27] We have made some experiments with adding a model of an arginine residue to the SO model system. However, the results are sensitive to where this group is placed (there are actually five arginine residues and one lysine within 10 Å of the Mo ion in SO[41]) and which restraints are used to fix it there (making the model specific for a certain protein and therefore not reflecting the intrinsic reactivity of the isolated active site). Moreover, the arginine model often transfers a proton to the sulfite ion, restoring the repulsion and giving a small effect on the barrier. Therefore, we decided to present energies only for the minimal active-site model. To obtain more reasonable barriers and unbiased results, QM/MM studies of specific enzymes are needed.

3.2.5. The DMSOR–SO_3^{2-} Reaction. Next, we studied whether the DMSOR model can oxidize sulfite to sulfate. The same five states (SR, TS1, IM, TS2, and SP) could be found also for the DMSOR model (Figure 4). The geometries of the various states for the two active-site models are quite similar. As shown in Table S11 in the Supporting Information, IM has closely similar Mo−OSO_3 and O−SO_3 bond lengths of 2.13 Å and 1.54−1.55 Å. However, TS1 is later for the DMSOR model, with a forming O−S bond of 2.26 Å compared to 2.51 Å for the SO model (but Mo−O = 1.78−1.80 Å in both cases). Likewise, TS2 is earlier, with a breaking Mo−O distance of 2.75 Å, compared to 3.60 Å for the DMSOR model.

The enthalpies of the five states are listed in Table 6. It can be seen that, for both active-site models, TS1 has the highest barrier and it is 10 kJ/mol higher for the DMSOR model, 177 compared to 167 kJ/mol. IM is less stable with the DMSOR model than with the native SO model (41 compared to 16 kJ/mol). On the other hand, the barrier for TS2 is appreciably lower. The reason for the latter is that the product state is appreciably more stable for the DMSOR model (−137 compared to −49 kJ/mol), as an effect of the intrinsic thermodynamic stability of the Mo(IV) state of the DMSOR model, as discussed in section 3.1.1.

dx.doi.org/10.1021/ic5010837 | *Inorg. Chem.* 2014, 53, 11913−11924

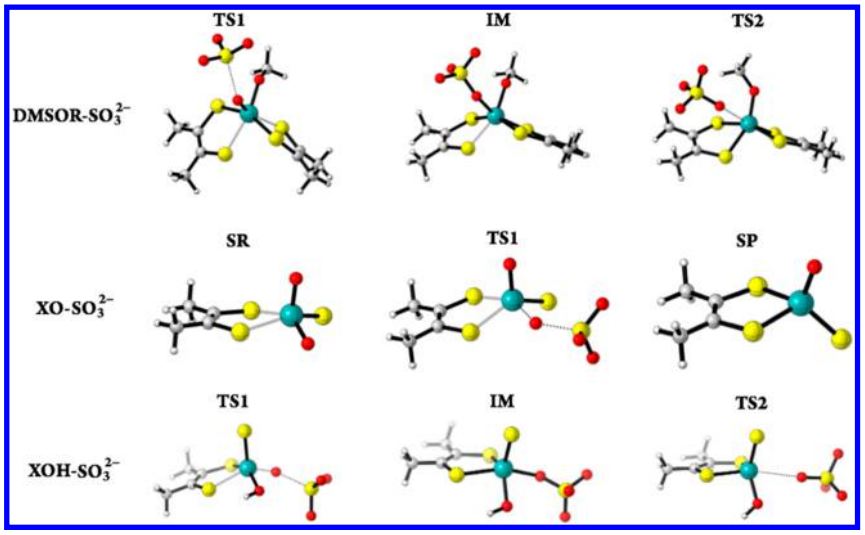

Figure 4. Structures of key states along DMSOR−SO_3^{2-}, XO−SO_3^{2-}, and XOH−SO_3^{2-} reactions obtained at the B3LYP-D2/def2-TZVPP+ZORA +COSMO level. For DMSOR−SO_3^{2-} and XOH−SO_3^{2-} reactions, TS1, IM, and TS2 are shown; for XO−SO_3^{2-}, only TS1 was located on the potential energy surface.

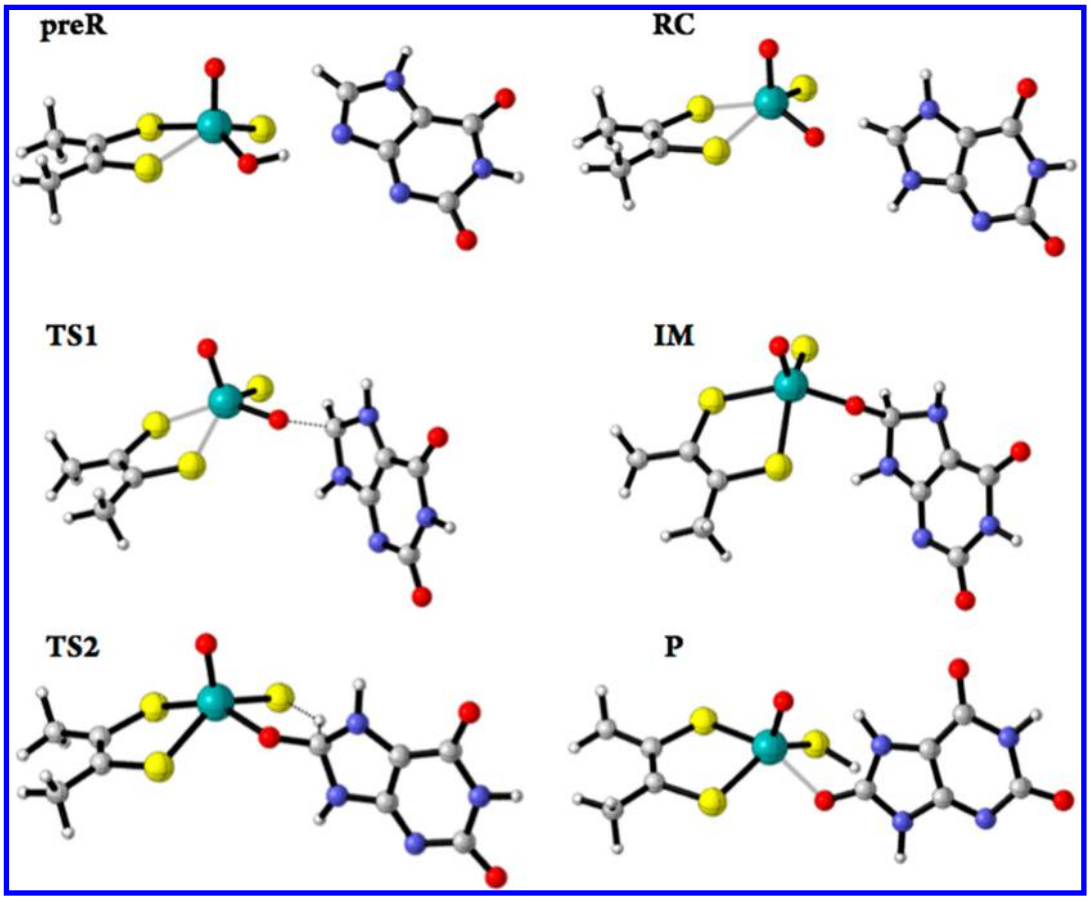

Figure 5. Structures of the various states along the XO−Xan reaction obtained at the B3LYP-D2/def2-TZVPP+ZORA+COSMO level.

3.2.6. The XO−SO_3^{2-} Reaction. Next, we consider the sulfite-oxidation reaction with the XO model. We first studied the reaction with the deprotonated $[MoO_2S(DMDT)]^{2-}$ model. However, the extra negative charge of this model strongly increased the Coulombic repulsion between the substrate and the active-site model to such an extent that neither IM nor TS2 could be found (Figure 4). Only TS1 was located, and it had an activation barrier of 455 kJ/mol, which is much higher than for the SO and DMSOR models.

Therefore, we instead studied the protonated XOH model. However, this is also somewhat problematic because, as Scheme 1 shows, XO has the OH^- ligand in an equatorial position and the oxy group at the apical position, whereas in the SO model, the reactive oxy group is in the equatorial position and QM studies have suggested that only that position is

dx.doi.org/10.1021/ic5010837 | Inorg. Chem. 2014, 53, 11913−11924

reactive.[26,71] This was solved by instead protonating the apical oxo group (but after optimization, the OH^- group moves to an equatorial position and instead the sulfido ligand moves to the apical position, as can be seen in Figure 4; still, it has an oxy group in the equatorial position, and it is only 2 kJ/mol less stable than the standard XOH model with the oxy group in the apical position). This XOH model gave a two-step mechanism closely similar to that of the SO model, as is shown in Table 6. The activation barrier is 183 kJ/mol, 16 and 6 kJ/mol larger than for the SO and DMSOR models. This shows that all three enzyme models probably can support a $SO_3^{2-} \rightarrow SO_4^{2-}$ reaction with fairly similar barriers (if the Coulomb repulsion can be overcome), although the native model gives the most reactive site.

3.2.7. The XO–Xan Reaction. Finally, we turned to the Xan → urate reaction. It has been extensively studied by several groups before,[3,7,31−3765] and we concentrated on the most favorable mechanism suggested by the thorough QM/MM study by Metz and Thiel:[36] It starts from the protonated oxidized active site with a hydroxide ion (XOH model) and a xanthine anion, protonated on the N_1 and N_7 atoms (called preR in Figure 5; in the original QM/MM study[36] this state was formed from neutral xanthine in its most stable protonation state by a deprotonation of N_3 by a nearby Glu residue, but the latter residue is not included in our cluster models, so it was skipped here; in the QM/MM study, the initial states had smaller activation barriers than the later steps considered here). Then, the proton of the OH^- group is transferred to the N_9 atom of xanthine, leading to the deprotonated XO model and a neutral xanthine in the second most stable protonation state (protonated on the N_1, N_7, and N_9 atoms), called RC. Next, the C–O bond is formed (IM) via a transition state TS1 with an elongated Mo–O distance (1.84 Å) and a partially formed O–C bond (1.75 Å). The calculated energy barrier is 62 kJ/mol (Table 6). In IM, the O–C bond is formed, but the transferred O atom still coordinates to the Mo center at a distance of 1.93 Å.

The third step is the transfer of the H_8 atom of xanthine to the sulfido ligand, overcoming a second, higher transition state TS2, which lies 44 kJ/mol above RC and 68 kJ/mol above preR. In TS2, the C–H_8 bond is elongated to 1.32 Å and the S–H_8 distance is 1.69 Å. Finally, the uric acid product is generated (**P**), which coordinates to the Mo center via the carbonyl group at the C_8 position, and 53 kJ/mol heat is released.

The predicted net activation barrier of 68 kJ/mol is in excellent agreement with the experimental value of 68 kJ/mol.[72] Our calculated energies are closely similar to those obtained by Metz and Thiel in their gas-phase reaction.[36] Analysis of the molecular orbitals clearly demonstrates that the oxidation state of the Mo center does not change during the first steps (RS → IM); the Mo ion is not reduced until the H_8 proton is transferred to the sulfido group.

3.2.8. The DMSOR–Xan and SO–Xan Reactions. Finally, we studied the Xan reaction with the DMSOR and SO models. Figure S1 in the Supporting Information shows the relaxed potential-energy surfaces along the C_8–O reaction coordinate (i.e., from RC toward IM) for these two models for neutral xanthine protonated on the N_1, N_3, and N_7 or the N_1, N_7, and N_9 atoms. It can be seen that the energies increase steadily, sometimes with a shoulder around 1.6 Å at energies of 103–118 kJ/mol (relative to RC). This indicates that the IM state does not exist (as was also confirmed by direct optimizations) for these models and the reaction cannot proceed.

We also made a similar scan with the intermediate model $[MoO(DMDT)(OH)(MeS)]^-$, which differs from the XOH model in that the sulfido ligand has been replaced by a MeS^- group. However, also for this model, no IM state could be found. Thus, we can conclude that only the XO model can catalyze the Xan → urate reaction. As the only difference between the XO and SO models is that the sulfido ligand is replaced by a MeS^- group, it seems that this sulfide ligand, or at least the double negative charge, is needed for the reaction.

To decide which of these effects is crucial, we also studied the model $[MoO_3(DMDT)]^{2-}$, in which we have replaced the sulfido ligand in the XO model by a third oxy group, keeping the double negative charge. Interestingly, the IM state could be found for this model, showing that the charge, rather than the chemical nature of this ligand, is most important. All six states in the XO–Xan reaction could also be found with this model (Figure 6). However, the barrier for the IM → P reaction (i.e., TS2) was prohibitively high, 128 kJ/mol relative to preR. Ilich and Hille, as well as Thiel and co-workers, have reached similar conclusions, replacing the sulfido ligand with an oxy group for the XO and aldehyde oxidoreductase reactions.[3,37,73,74] They explain the higher barrier with more severe geometrical requirements in the hydride-transfer transition state with the oxy group. This high barrier is in accordance with the experimental observation that the desulfo form of XO is inactive,[75,76] although kinetic, spectroscopic, and crystallographic studies indicate that the related aldehyde oxidoreductase enzyme is active without the sulfido group.[77] Kirk and co-workers have emphasized the role of the sulfido ligand for the proper electronic structure of the transition state for the hydride-transfer reaction.[78,79] Thus, we can conclude that the XO active site is carefully designed to make all three steps in the reaction mechanism possible: a proper acidity to make the initial proton transfer possible, a favorable net charge to enable the oxy transfer, and again a proper acidity to make the hydride transfer feasible. No native or designed enzyme model combines these properties as well as the XO model. In

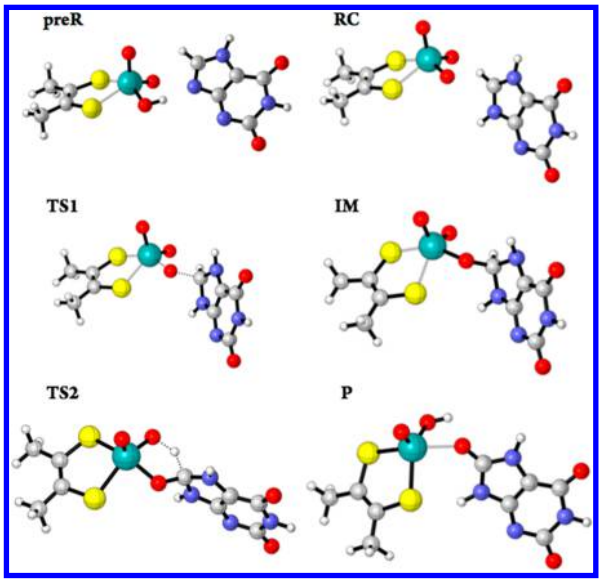

Figure 6. Structures of the various states along the $[MoO_3(DMDT)]^{2-}$–Xan reaction.

dx.doi.org/10.1021/ic5010837 | *Inorg. Chem.* 2014, 53, 11913–11924

particular, the sulfido group seems crucial for the properties of the XO site.

4. CONCLUSIONS

We have explored the active-site design of typical examples of the three families of mononuclear molybdenum OAT enzymes, DMSOR, SO, and XO, using the B3LYP method. The effect of the enzyme environment on the energy surfaces has been modeled by the COSMO continuum-solvent model with a dielectric constant of 4 without any introduction of residues at the active site, but including dispersion corrections.

This theoretical study offers important thermodynamic and kinetic clues to the understanding of why the three families use different Mo ligands in their active sites. We have shown that the various enzyme models have differing oxidizing powers; the DMSOR model with its two DMDT ligands gives the largest oxidizing power, although it performs a reduction reaction. The reason for this seems to be to save energy: the ligands have been selected to give a reaction free energy close to zero. This facilitates the regeneration of the active site after the OAT reaction by electron- and proton-transfer reactions. The Mo ligands seem to have been selected so that the DMSOR site can be rereduced, whereas the SO and XO sites instead can be reoxidized after the oxo-transfer reaction has been performed.

Moreover, we have studied a typical reaction of each member of the three families, the reduction of DMSO to DMS, the oxidation of sulfite to sulfate, and the oxidation of xanthine to uric acid. We have studied the reactions, not only with the native enzyme models but also with models of the other two enzyme families. These calculations showed that the DMSOR reaction is facile and can be performed also with the SO and XO models, which actually give lower activation barriers, owing to their more exothermic reaction energies. Likewise, the DMSOR and XO models can perform the oxidation of sulfite, provided that the Coulombic repulsion between the substrate and the active-site model can be overcome. However, in this case, the native model gives the lowest activation energy. On the other hand, XO is the only model that can oxidize xanthine. In particular, the sulfido group with its double negative charge seems to be necessary for this reaction. In conclusion, these calculations give important clues to how Nature has designed the various families of OAT enzymes.

■ ASSOCIATED CONTENT

Supporting Information

Energies and geometries optimized at the B3LYP/def2-TZVPP level of theory. This material is available free of charge via the Internet at http://pubs.acs.org.

■ AUTHOR INFORMATION

Corresponding Author

*E-mail: Ulf.Ryde@teokem.lu.se. Tel: +46-46 222 45 02. Fax: +46-46 222 86 48.

Notes

The authors declare no competing financial interest.

■ ACKNOWLEDGMENTS

This work has been supported by grants from the Swedish Research Council (Project 2010-5025) and the Crafoord Foundation, as well as by computer resources of Lunarc at Lund University. It has also supported by the National Basic Research Program of China (973 Program, 2012CB932800) and National Natural Science Foundation of China (NSFC No. 21103064).

■ REFERENCES

(1) Kaim, W.; Schwederski, B. *Bioionorganic chemistry: Inorganic elements in the chemistry of life*; J. Wiley & Sons: Chichester, 1991.
(2) Holm, R. H.; Solomon, E. I.; Majumdar, A.; Tenderholt, A. *Coord. Chem. Rev.* **2011**, *255*, 993−1015.
(3) Metz, S.; Thiel, W. *Coord. Chem. Rev.* **2011**, *255*, 1085−1103.
(4) Hille, R. *Chem. Rev.* **1996**, *96*, 2757−2816.
(5) Romao, M. J.; Knablein, J.; Huber, R.; Moura, J. J. *Prog. Biophys. Mol. Biol.* **1997**, *68*, 121−144.
(6) Rajapakshe, A.; Astashkin, A. V.; Klein, E. L.; Reichmann, D.; Mendel, R. R.; Bittner, F.; Enemark, J. H. *Biochemistry* **2011**, *50*, 8813−8822.
(7) Schwarz, G.; Mendel, R. R. *Annu. Rev. Plant Biol.* **2006**, *57*, 623−647.
(8) Das, S. K.; Chaudhury, P. K.; Biswas, D.; Sarkar, S. *J. Am. Chem. Soc.* **1994**, *116*, 9061−9070.
(9) Thapper, A.; Deeth, R. J.; Nordlander, E. *Inorg. Chem.* **1999**, *38*, 1015−1018.
(10) Lim, B. S.; Sung, K. M.; Holm, R. H. *J. Am. Chem. Soc.* **2000**, *122*, 7410−7411.
(11) Smith, P. D.; Millar, A. J.; Young, C. G.; Ghosh, A.; Basu, P. *J. Am. Chem. Soc.* **2000**, *122*, 9298−9299.
(12) Webster, C. E.; Hall, M. B. *J. Am. Chem. Soc.* **2001**, *123*, 5820−5821.
(13) Thapper, A.; Deeth, R. J.; Nordlander, E. *Inorg. Chem.* **2002**, *41*, 6695−6702.
(14) McNamara, J. P.; Joule, J. A.; Hillier, I. H.; Garner, C. D. *Chem. Commun.* **2005**, 177−179.
(15) McNamara, J. P.; Hillier, I. H.; Bhachu, T. S.; Garner, C. D. *Dalton Trans.* **2005**, 3572−3579.
(16) Hille, R. *Arch. Biochem. Biophys.* **2005**, *433*, 107−116.
(17) Hofmann, M. *Inorg. Chem.* **2008**, *47*, 5546−5548.
(18) Hernandez-Marin, E.; Ziegler, T. *Can. J. Chem.* **2010**, *88*, 683−693.
(19) Tenderholt, A. L.; Wang, J. J.; Szilagyi, R. K.; Holm, R. H.; Hodgson, K. O.; Hedman, B.; Solomon, E. I. *J. Am. Chem. Soc.* **2010**, *132*, 8359−8371.
(20) Li, J. L.; Mata, R. A.; Ryde, U. *J. Chem. Theory Comput.* **2013**, *9*, 1799−1807.
(21) Sung, K. M.; Holm, R. H. *J. Am. Chem. Soc.* **2001**, *123*, 1931−1943.
(22) Mohr, M.; McNamara, J. P.; Wang, H.; Rajeev, S. A.; Ge, J.; Morgado, C. A.; Hillier, I. H. *Faraday Discuss.* **2003**, *124*, 413.
(23) Tenderholt, A. L.; Hodgson, K. O.; Hedman, B.; Holm, R. H.; Solomon, E. I. *Inorg. Chem.* **2012**, *51*, 3436−3442.
(24) Hofmann, M. *J. Mol. Struct.: THEOCHEM* **2006**, *773*, 59−70.
(25) Hille, R. *Biochim. Biophys. Acta, Bioenerg.* **1994**, *1184*, 143−169.
(26) van Severen, M.-C.; Andrejić, M.; Li, J.; Starke, K.; Mata, R. A.; Nordlander, E.; Ryde, U. *J. Biol. Inorg. Chem.* **2014**, *19*, 1165−1179.
(27) Hernandez-Marin, E.; Ziegler, T. *Inorg. Chem.* **2009**, *48*, 1323−1333.
(28) Pal, K.; Chaudhury, P. K.; Sarkar, S. *Chem.—Asian J.* **2007**, *2*, 956−964.
(29) Wilson, H. L.; Rajagopalan, K. V. *J. Biol. Chem.* **2004**, *279*, 15105−15113.
(30) Harrison, R. *Free Radical Biol. Med.* **2002**, *33*, 774−797.
(31) Amano, T.; Ochi, N.; Sato, H.; Sakaki, S. *J. Am. Chem. Soc.* **2007**, *129*, 8131−8138.
(32) Bayse, C. A. *Dalton Trans.* **2009**, 2306−2314.
(33) Zhang, X. H.; Wu, Y. D. *Inorg. Chem.* **2005**, *44*, 1466−1471.
(34) Doonan, C. J.; Stockert, A.; Hille, R.; George, G. N. *J. Am. Chem. Soc.* **2005**, *127*, 4518−4522.
(35) Alfaro, J. F.; Jones, J. P. *J. Org. Chem.* **2008**, *73*, 9469−9472.
(36) Metz, S.; Thiel, W. *J. Am. Chem. Soc.* **2009**, *131*, 14885−14902.
(37) Metz, S.; Thiel, W. *J. Phys. Chem. B* **2010**, *114*, 1506−1517.

(38) Page, C. C.; Moser, C. C.; Chen, X.; Dutton, P. L. *Nature* **1999**, *402*, 47−52.
(39) Stockert, A. L.; Shinde, S. S.; Anderson, R. F.; Hille, R. *J. Am. Chem. Soc.* **2002**, *124*, 14554−14555.
(40) Schopfer, L. M.; Massey, V.; Nishino, T. *J. Biol. Chem.* **1988**, *263*, 13528−13538.
(41) Li, H.-K.; Temple, C.; Rajagopalan, K. V.; Schindelin, H. *J. Am. Chem. Soc.* **2000**, *122*, 7673−7680.
(42) Kisker, C.; Schindelin, H.; Pacheco, A.; Wehbi, W. A.; Garrett, R. M.; Rajagopalan, K. V.; Enemark, J. H.; Rees, D. C. *Cell* **1997**, *91*, 973−983.
(43) Pauff, J. M.; Cao, H.; Hille, R. *J. Biol. Chem.* **2009**, *284*, 8760−8767.
(44) Neese, F. *WIREs Comput. Mol. Sci.* **2012**, *2*, 73−78.
(45) Becke, A. D. *J. Chem. Phys.* **1993**, *98*, 5648−5652.
(46) Kim, K.; Jordan, K. D. *J. Phys. Chem.* **1994**, *98*, 10089−10094.
(47) Siegbahn, P. E. M.; Borowski, T. *Acc. Chem. Res.* **2006**, *39*, 729−738.
(48) Tao, J.; Perdew, J. P.; Staroverov, V. N.; Scuseria, G. E. *Phys. Rev. Lett.* **2003**, *91*, 146401.
(49) Weigend, F.; Ahlrichs, R. *Phys. Chem. Chem. Phys.* **2005**, *7*, 3297−3305.
(50) Neese, F.; Wennmohs, F.; Hansen, A.; Becker, U. *Chem. Phys.* **2009**, *356*, 98−109.
(51) van Lenthe, E.; Ehlers, A.; Baerends, E. J. *J. Chem. Phys.* **1999**, *110*, 8943−8953.
(52) Grimme, S. *J. Comput. Chem.* **2006**, *27*, 1787−1799.
(53) Klamt, A.; Schüürmann, G. *J. Chem. Soc., Perkin Trans.* **1993**, *2*, 799−805.
(54) Klamt, A.; Jonas, V.; Bürger, T.; Lohrenz, J. C. W. *J. Phys. Chem. A* **1998**, *102*, 5074−5085.
(55) Cossi, M.; Tomasi, J.; Cammi, R. *Int. J. Quantum Chem.* **1995**, *56*, 695−702.
(56) Miertus, S.; Scrocco, E.; Tomasi, J. *Chem. Phys.* **1981**, *55*, 117−129.
(57) Tomasi, J.; Mennucci, B.; Cammi, R. *Chem. Rev.* **2005**, *105*, 2999−3094.
(58) Frisch, M. J.; Trucks, G. W.; Schlegel, H. B.; Scuseria, G. E.; Robb, M. A.; Cheeseman, J. R.; Montgomery, J. A., Jr.; Vreven, T.; Kudin, K. N.; Burant, J. C.; Millam, J. M.; Iyengar, S. S.; Tomasi, J.; Barone, V.; Mennucci, B.; Cossi, M.; Scalmani, G.; Rega, N.; Petersson, G. A.; Nakatsuji, H.; Hada, M.; Ehara, M.; Toyota, K.; Fukuda, R.; Hasegawa, J.; Ishida, M.; Nakajima, T.; Honda, Y.; Kitao, O.; Nakai, H.; Klene, M.; Li, X.; Knox, J. E.; Hratchian, H. P.; Cross, J. B.; Adamo, C.; Jaramillo, J.; Gomperts, R.; Stratmann, R. E.; Yazyev, O.; Austin, A. J.; Cammi, R.; Pomelli, C.; Ochterski, J. W.; Ayala, P. Y.; Morokuma, K.; Voth, G. A.; Salvador, P.; Dannenberg, J. J.; Zakrzewski, V. G.; Dapprich, S.; Daniels, A. D.; Strain, M. C.; Farkas, O.; Malick, D. K.; Rabuck, A. D.; Raghavachari, K.; Foresman, J. B.; Ortiz, J. V.; Cui, Q.; Baboul, A. G.; Clifford, S.; Cioslowski, J.; Stefanov, B. B.; Liu, G.; Liashenko, A.; Piskorz, P.; Komaromi, I.; Martin, R. L.; Fox, D. J.; Keith, T.; Al-Laham, M. A.; Peng, C. Y.; Nanayakkara, A.; Challacombe, M.; Gill, P. M. W.; Johnson, B.; Chen, W.; Wong, M. W.; Gonzalez, C.; Pople, J. A. *Gaussian 03, revision E.01*; Gaussian Inc.: Wallingford, CT, 2004.
(59) Ryde, U.; Mata, R. A.; Grimme, S. *Dalton Trans.* **2011**, *40*, 11176−11183.
(60) Kelly, C. P.; Cramer, C. J.; Truhlar, D. G. *J. Phys. Chem. B* **2006**, *110*, 16066−16081.
(61) Heimdal, J.; Kaukonen, M.; Srnec, M.; Rulíšek, L.; Ryde, U. *ChemPhysChem* **2011**, *12*, 3337−3347.
(62) Holm, R. H. *Chem. Rev.* **1987**, *87*, 1401−1449.
(63) Holm, R. H.; Donahue, J. P. *Polyhedron* **1993**, *12*, 571−589.
(64) Lee, S. C.; Holm, R. H. *Inorg. Chim. Acta* **2008**, *361*, 1166−1176.
(65) Hille, R. *Eur. J. Inorg. Chem.* **2006**, *2006*, 1913−1926.
(66) Dunitz, J. D. *Science* **1994**, *264*, 670.
(67) Rulíšek, L.; Jensen, K. P.; Lundgren, K.; Ryde, U. *J. Comput. Chem.* **2006**, *27*, 1398−1414.
(68) Irudayam, S. J.; Henchman, R. H. *J. Phys. Chem. B* **2009**, *113*, 5871−5884.
(69) Cobb, N.; Hemann, C.; Polsinelli, G. A.; Ridge, J. P.; McEwan, A. G.; Hille, R. *J. Biol. Chem.* **2007**, *282*, 35519−35529.
(70) Majumdar, A.; Sarkar, S. *Coord. Chem. Rev.* **2011**, *255*, 1039−1054.
(71) Peariso, K.; McNaughton, R. L.; Kirk, M. L. *J. Am. Chem. Soc.* **2002**, *124*, 9006−9007.
(72) Yamaguchi, Y.; Matsumura, T.; Ichida, K.; Okamoto, K.; Nishino, T. *J. Biochem.* **2007**, *141*, 513−524.
(73) Metz, S.; Wang, D.; Thiel, W. *J. Am. Chem. Soc.* **2009**, *131*, 4628−4640.
(74) Ilich, P.; Hille, R. *J. Am. Chem. Soc.* **2002**, *124*, 6769−6770.
(75) Massey, V.; Edmondson, D. *J. Biol. Chem.* **1970**, *245*, 6595−6598.
(76) Nishino, T.; Usami, C.; Tsushima, K. *Proc. Natl. Ac. Sci. U.S.A.* **1983**, *80*, 1826−1829.
(77) Santos-Silva, T.; Ferroni, F.; Thapper, A.; Marangon, J.; González, P. J.; Rizzi, A. C.; Moura, I.; Moura, J. J. G.; Romão, M. J.; Brondino, C. D. *J. Am. Chem. Soc.* **2009**, *131*, 7990−7998.
(78) Sempombe, J.; Stein, B.; Kirk, M. L. *Inorg. Chem.* **2011**, *50*, 10919−10928.
(79) Kirk, M. L.; Berhane, A. *Chem. Biodiversity* **2012**, *9*, 1756−1760.